JGR Atmospheres

RESEARCH ARTICLE
10.1029/2019JD031254

A Bayesian-Like Approach to Describe the Regional Variation of High-Flash Rate Thunderstorms From Thermodynamic and Kinematic Environment Variables

Nana Liu[1], **Chuntao Liu**[1], **and Philippe E. Tissot**[1,2]

[1]Department of Physical and Environmental Sciences, Texas A&M University at Corpus Christi, Corpus Christi, TX, USA, [2]Conrad Blucher Institute, Texas A&M University at Corpus Christi, Corpus Christi, TX, USA

Key Points:
- Sole environmental factor has limited skill to estimate the probability of high-flash rate thunderstorms
- A combination of four variables can be used to derive a geographical distribution of high-flash rate events by a Bayesian-like approach
- The strong land-ocean contrast in the frequency of high-flash rate thunderstorms can be closely reproduced from the reanalysis data

Correspondence to:
N. Liu,
nliu@islander.tamucc.edu

Citation:
Liu, N., Liu, C., & Tissot, P. E. (2019). A Bayesian-like approach to describe the regional variation of high-flash rate thunderstorms from thermodynamic and kinematic environment variables. *Journal of Geophysical Research: Atmospheres*, *124*, 12,507–12,522. https://doi.org/10.1029/2019JD031254

Received 27 JUN 2019
Accepted 6 NOV 2019
Accepted article online 11 NOV 2019
Published online 3 DEC 2019

Abstract A 16-year Tropical Rainfall Measuring Mission convective feature (CF) data set and ERA-Interim reanalysis data are used to examine the nonlinear relationships between thermodynamic environments and the probability of high-flash rate thunderstorms. First, Bayesian-like probability functions are established between preselected ERA-Interim thermodynamic variables and the high-flash rate CFs. Then, the global geographical distribution of high-flash rate thunderstorms is validated by applying these functions to the reanalysis data. The results suggest that a sole environmental factor has limited skill to estimate the probability of these events. The combination of four variables, including Convective Available Potential Energy, convection inhibition, low-level shear, and warm cloud depth, may be used to derive a geographical distribution of high-flash rate events that is close to the observations. The strong land-ocean contrast in the frequency of high-flash rate thunderstorms and some hot spot regions can be closely reproduced based only on these four variables from the reanalysis data. This indicates that the land-ocean contrast in the occurrence of high-flash rate thunderstorms can be largely interpreted by the fundamental differences between the thermodynamic conditions over land and ocean.

1. Introduction

Extreme weather events are increasingly drawing our attention due to a growing concern that they will have an increasing impact on humans and societies, no matter where they occur, exacerbated by natural and anthropogenic climate change. Despite continuous improvements in observation and modeling tools, the prediction of these events, especially of intense ones, remains a considerable challenge (Gallus et al., 2005). The prediction of extreme weather events that produce significant amounts of lightning continues to be a difficult task and a fascinating scientific challenge because they occur in a wide range of weather regimes and have various sizes and lifetimes (e.g., Feng et al., 2016; Foote & Mohr, 1979; Wilson et al., 1998).

While numerical models have proven useful in improving our understanding of thunderstorms in the atmosphere, operational numerical models, with a horizontal grid spacing of about 10 km, have often failed to predict not only the location and time of convective initiation (Anquetin et al., 2005; Meißner et al., 2007) but also the type and intensity of thunderstorms (e.g., Kain et al., 2013; Mecikalski et al., 2015; Romero et al., 2015). Alternatively, the statistical approach of meteorological covariates can be used to investigate the occurrence of these extreme events (Brooks et al., 2003; Brown & Murphy, 1996). Covariates relate environmental conditions that are well observed in space and time to the weather events of interest. This method has led to many of the current forecasting approaches for intense thunderstorms. For example, proximity soundings, where observations from radiosondes are taken in the vicinity of tornadoes, have been used to understand environmental conditions associated with tornadoes (Rasmussen & Blanchard, 1998). Parameters calculated from sounding data are widely used to identify the preconvective environments that favor intense thunderstorms. These parameters and indices generally reflect the potential for the development of intense thunderstorms, making it possible to quantify the uncertainty implicit in any forecast (Kaltenböck et al., 2009; Murphy, 1977).

In the past decades, various thermodynamic and kinematic parameters have been designed to characterize the conditions that could favor the formation and development of thunderstorms.

As a forecasting tool for gauging the likelihood of intense thunderstorms, Convective Available Potential Energy (CAPE) is frequently used in past studies. This is because the relative motion of hydrometeors inside the cloud depends on the updraft speed. The strength of updraft is directly related to the vertical profile of CAPE (Blanchard, 1998; Doswell & Evans, 2003; Doswell & Rasmussen, 1994). CAPE has also been used in cumulus parameterizations in general circulation models (e.g., Moncrieff & Miller, 1976; Washington & Parkinson, 2005; Ye et al., 1998) and as a predictor of lightning intensity in deep tropical convection (Williams et al., 1992). As a complementary parameter to CAPE, convection inhibition (CIN) is another variable that plays an important role in the development of intense convection (e.g., Davies, 2004; Mapes, 1998; Stensrud, 2007). Convection is often widespread but shallow in the absence of CIN (Bennett et al., 2006). The presence of CIN can allow for the accumulation of heat and moisture, creating the potential for intense convection. In addition to CAPE and CIN, low-level wind shear has also gained wide acceptance by the forecaster community as a parameter to identify potential intense weather (Rotunno et al., 1988; Weisman & Rotunno, 2004). Weisman and Klemp (1986) suggested that the bulk Richardson number, which combines CAPE and surface to 6-km wind shear, can be used to differentiate storm type, organization, and lifetime. Since then, many researchers have used proxies that combine CAPE and wind shear to model the occurrence of intense convection (e.g., Allen et al., 2015; Diffenbaugh et al., 2013; Sander et al., 2013).

Williams et al. (2005) present that an elevated cloud base height may increase the cloud water concentration in the mixed-phase region. This is important because the presence of ice particles in this region is necessary for cloud electrification (e.g., Houze, 1993; MacGorman & Rust, 1998; Takahashi, 1978). Higher cloud base height could result in less entrainment (McCarthy, 1974), stronger updrafts (Williams et al., 2005), and ultimately, higher liquid water content in the mixed-phase zone. In addition, a higher cloud base height also implies a shallower warm cloud depth (WCD), which is the distance between the cloud base height and freezing height. A shallower WCD allows less time for droplets to interact for coalescence (Pierce, 1958) and results in a higher liquid water content in the mixed-phase and charging zone from the freezing of large raindrops (Rosenfeld & Woodley, 2003). Stolz et al. (2015) also confirmed that lightning density and the average height of 30-dBZ echoes are higher for storms with a shallower WCD, compared to those with a deeper WCD. In their multiple linear regression model to predict global lightning activity, they suggested that WCD, CAPE, and cloud condensation nuclei are among the most influential predictors accounting for the variation of convective intensity (Stolz et al., 2017).

In addition to the thermodynamic and kinematic factors above, other parameters have been used in the past to evaluate the potential for intense convection, including low- and middle-level humidity (e.g., Manzato, 2012; Sherwood et al., 2010; Wissmeier & Goler, 2009), lifted index (LI_{500}, e.g., Galway, 1956; Manzato, 2012; Xia et al., 2018), and total column water vapor (TCWV, e.g., Holloway & Neelin, 2009; Schiro et al., 2016; Tompkins & Semie, 2017). Although these parameters may influence convective activity in different ways, no parameter could characterize the state of the atmosphere on its own. Therefore, this study explores the influence of these parameters/factors individually and jointly on the probability of intense thunderstorms.

In past investigations of intense thunderstorms, satellites have provided valuable information about the global distribution of intense convection (e.g., Cecil & Blankenship, 2012; Liu & Liu, 2016; Spencer & Santek, 1985; Zipser et al., 2006). The near-uniform global coverage of satellites makes them continue to be the most efficient tools to advance the understanding of extreme weather events. As one of the most successful missions during the past decades, the Tropical Rainfall Measuring Mission (TRMM, Kummerow et al., 1998) has provided us a clear picture of the distribution of thunderstorms and lightning activity across the tropics and subtropics (Albrecht et al., 2016; Houze et al., 2015; Liu & Zipser, 2005; Zipser et al., 2006). In order to describe the regional variation of thunderstorms from the perspective of thermodynamic environments, here we focus on the large-scale thermodynamic environments from reanalysis data sets for intense convective systems observed by TRMM.

The objective of this study is to investigate the relationships between the thermodynamic variables such as CAPE, CIN, and low-level wind shear individually as well as jointly and the probability of intense thunderstorms. Then, these relationships are used to interpret the global geographical frequency distribution of intense thunderstorms. With this objective, lightning flashes, a commonly used proxy to recognize intense thunderstorms (e.g., Carey et al., 2003; Lang & Rutledge, 2002; MacGorman & Burgess, 1994), are used to

Table 1
Percentage of CFs With More Than 50 Flashes and Mean and Standard Deviation of Selected Intensity Proxies for Those CFs Over Land and Ocean

	Percentage of high-flash rate CFs (%)	Maximum 40-dBZ echo tops (km)	Minimum PCT at 85 GHz (K)	Minimum PCT at 37 GHz (K)	Convective precipitation area (km^2)
Land	0.38	10.7 ± 2.2	111 ± 29	211 ± 24	3,439 ± 3,083
Ocean	0.02	9.9 ± 1.9	103 ± 25	205 ± 24	4,057 ± 3,102

identify these rare events. The lightning flashes are observed by the Lightning Imaging Sensor (LIS) on the TRMM satellite. The LIS provided 16+ years of continuous total lightning observations with high detection efficiency across the tropics and subtropics after its launch in 1997. The 16 years of TRMM data and analysis methodology used in this study are introduced in section 2. The results are presented in section 3, which includes the relationships between several selected atmospheric factors and the occurrence of intense thunderstorms, the reconstructed geographical distribution and seasonal variation of those events predicted by these relationships, and the relative importance of these atmospheric variables over selected regions.

2. Data and Methods

Two data sources are used in this study to investigate the occurrence of intense thunderstorms based on their relationship to atmospheric variables. One is the database of TRMM convective features (CFs) and their properties. In addition, the ERA-Interim reanalysis data (Dee et al., 2011) are used to calculate the thermodynamic variables for each CF.

2.1. TRMM Feature Data Sets

The study uses a 16-year (1998–2013) CF data set that is derived from the TRMM version 7 products, with a coverage of 36°S–36°N. A CF is defined by grouping contiguous convective precipitation pixels observed by the TRMM Precipitation Radar (Liu et al., 2008). In this analysis, only CFs with at least four contiguous pixels (with size ~75 km^2) are used, in order to limit the noise. CFs with at least four contiguous pixels are hereafter referred to as CFs. The LIS detects both cloud-to-ground and intracloud lightning activity within ~92 s of the overpass time after the boost of the satellite orbit in August of 2001 (Albrech et al., 2011). Each LIS lightning flash is assigned to the nearest Precipitation Radar pixel. Then, the lightning flash count is summarized for each CF. Having collected lightning measurements for over 16 years, LIS has been especially useful in the effort to understand lightning activity in remote regions of the world that have limited ground-based observations (Cecil et al., 2014; Virts et al., 2013; Zipser et al., 2006).

A total of ~25 million CFs from 16-year TRMM observations are used in this study. The large sample size of CFs over the TRMM domain makes it possible to examine these rare events across the tropics and subtropics. With a focus on convection that produces intense weather, we define CFs with more than 50 flashes (≥32 flashes/min; about the top 0.38% flash rate over land and 0.02% over ocean) as intense thunderstorms in this study. To verify that the CFs with more than 50 flashes are indeed intense, mean values of a few other proxies for convective intensity, including the maximum 40-dBZ echo top height and minimum brightness temperature at the 85- and 37-GHz channels, are listed in Table 1. CFs with more than 50 flashes are mostly mesoscale convective systems with large precipitating area (>3,000 km^2). These CFs have mean maximum 40-dBZ echo top height greater than ~10 km and mean minimum 85-GHz PCT less than 112 K over both land and ocean. Events with 40-dBZ echo tops reaching 10 km are the most extreme top 0.1% of precipitating features in Zipser et al. (2006). Wu et al. (2016) and Houze et al. (2015) also used 10-km 40-dBZ echo top height as the criteria for the most intense convection over the Himalayas. Therefore, though the criterion of 50 flashes in this study is arbitrary, the selected CF events are verified as intense by other convective intensity proxies.

As shown in Figure 1, thunderstorms, especially intense ones, exhibit a strong preference for formation near major mountain ranges, such as the east of the Rockies and Andes, south of the Himalayas, and the west of the Mitumba mountain (Figure 1b). This is similar to the climatology map of intense thunderstorms depicted by prior studies (e.g., Mohr & Zipser, 1996; Zipser et al., 2006; Cecil & Blankenship, 2012; Matsui et al., 2016). As noted in Figure 1a, more CFs are sampled in subtropical latitudes due to the low inclination orbit. Here

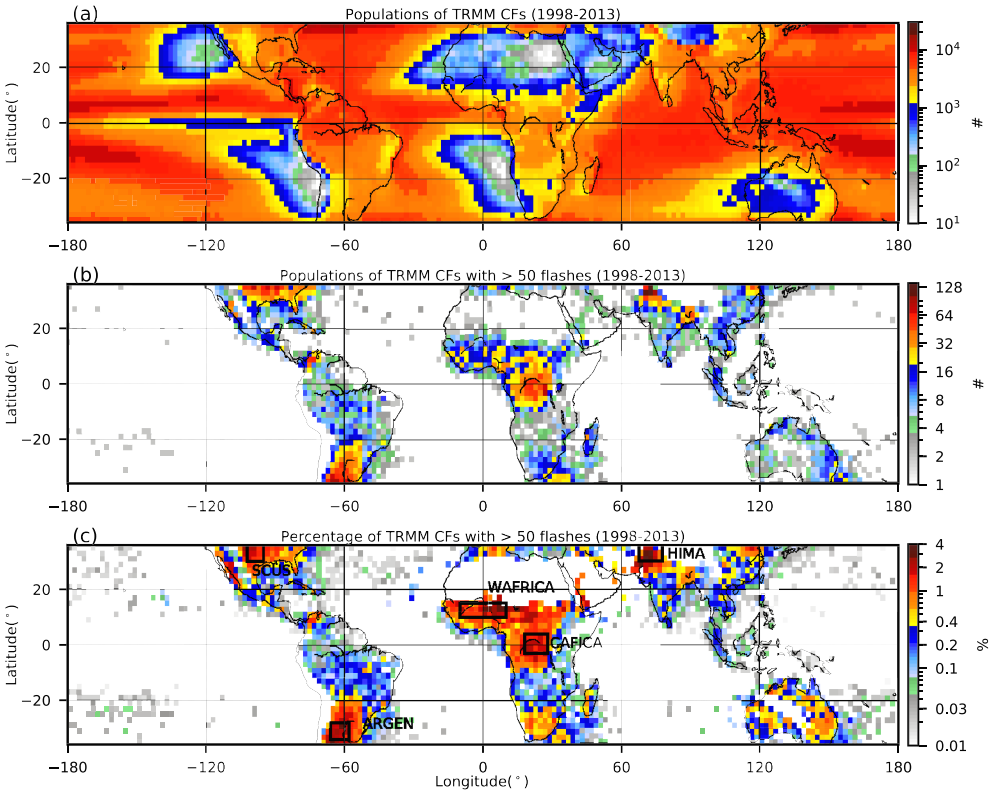

Figure 1. (a) Geographical distribution of the population of TRMM CFs. (b) Geographical distribution of the population of TRMM CFs with more than 50 flashes. (c) Geographical distribution of the percentage of TRMM CFs with more than 50 flashes; boxes with less than 500 CFs have been left blank. The distribution is created on a 2° × 2° grid from 16 years (1998–2013) of TRMM observations.

we are interested in the likelihood of high-flash rate thunderstorms under specific thermodynamic and kinematic environments. Therefore, we focus on the probability of a CF being intense under different environments. In each 2° × 2° grid, the percentage of intense CFs is defined as the number of CFs with more than 50 flashes divided by the total number of CFs with at least four contiguous pixels, multiplied by 100 (%). The geographical distribution of the percentage of intense CFs (those with more than 50 flashes) is shown in Figure 1c. Similar to the population distribution in Figure 1b, a higher percentage of intense CFs is found over land than over ocean, with a strong preference over several specific regions, such as Argentina, Congo, Northern Pakistan, and the south central United States, which is consistent with Zipser et al. (2006).

2.2. Thermodynamic Environments From ERA-Interim Reanalysis Data Set

The 0.75° resolution 6 hourly ERA-Interim reanalysis data (Dee et al., 2011) are used to provide the large-scale thermodynamic environments for each TRMM-identified intense CF. The base-state variables used in this study include fields of temperature (T), horizontal wind (u and v), geopotential heights, relative humidity (RH) at 37 pressure levels, and 2-m temperature. First, these fields are temporally interpolated to the CF time from 6 hourly ERA-Interim data. Then, the nearest profile to the CF is chosen from the 0.75° × 0.75° grids. For each CF, 10 levels of the atmospheric profiles are selected from the original 37 levels (Liu et al., 2008).

Additionally, a few other parameters are derived from these base-state variables. CAPE and CIN are computed using the algorithms outlined by Emanuel (1994). They are the areas enclosed between the environmental temperature profile and the path of a rising air parcel between two specific height levels. The positive area between the level of free convection and the level of neutral buoyancy is defined as CAPE, while the negative area between the level of lifting and the level of free convection is defined as CIN. The most unstable CAPE (hereinafter referred to as CAPE) is used in this study. It is calculated by lifting

parcels from multiple pressure levels between the surface and about 700 hPa and finding the highest CAPE value. The low-level wind shear ($SHEAR_{1-3\ km}$) is defined as the difference in the horizontal wind between 1 and 3 km above ground level. The WCD is calculated by subtracting the lifting condensation level (LCL) from the freezing level (height of the 0 °C isotherm). The specific humidity at the near surface (SHL) is calculated from the 2-m dew point temperature and surface pressure, while the relative humidity at the middle level (RHM) is averaged over the 700- to 500-hPa layer. Then, these parameters are temporally and spatially interpolated to the time and location of each CF. The lifted index (LI_{500}) is calculated as the difference between the environmental temperature and the temperature of a rising air parcel at 500 hPa.

All of these arbitrarily selected variables reflect certain corresponding physical processes, though some of them are more often employed in data analysis, while others are more often employed in modeling contexts, mostly due to historical as well as practical reasons. Note that all of these variables can be both calculated from observations, if the relevant atmospheric variables are properly measured, or obtained from the model outputs.

2.3. Bayesian-Like Models to Describe the Regional Variation of Thunderstorms

Because CFs with more than 50 flashes have large areas that are likely in excess of an ERA-Interim grid box, they are unlikely to coexist with nonintense CFs within the same ERA-Interim grid. We assume that intense and nonintense thunderstorms are mutually exclusive for this analysis. In other words, these two types of events do not occur at the same time under the same environments. In the Bayesian-like model, the probability of intense thunderstorms can be denoted as P (intense thunderstorms|C), where C is a condition with a predictor variable, such as CAPE and CIN. The approach is to use equation (1) to calculate the probability of intense thunderstorms.

$$P(\text{intense thunderstorms}|C) = \frac{P(\mathrm{CF_{fl50}}|C)}{P(\mathrm{CF_{All}}|C)}, \tag{1}$$

where P (intense thunderstorms| C) is the probability of intense thunderstorms under the condition (C) with a value of a certain predictor variable. P ($\mathrm{CF_{fl50}}|C$) is the number of CFs with more than 50 flashes under the condition C, while P ($\mathrm{CF_{All}}|C$) is the number of total CFs under the same condition (C). Here the condition C refers to a grid point with surface precipitation and a specific large-scale environment, such as a value of CAPE and CIN or a combination of two or more variables as an environmental condition associated with the probability of intense thunderstorms. Here, two methods are considered. The first one explores the relationship between atmospheric variables and the probability of intense CFs based on CFs over the whole TRMM domain (36°S–36°N), including both land and ocean. The second considers the land and ocean separately for the analysis. Then, the probability of intense thunderstorms calculated by the Bayesian-like model is used to reconstruct their geographical distribution from atmospheric variables from ERA-Interim to better understand the regional and seasonal variation of these events.

3. Results

3.1. Relationships Between Thermodynamic Variables and Probability of Intense CFs

The relationship between one specific atmospheric variable and the percentage of CFs with more than 50 flashes is shown in Figure 2. The percentage is calculated as the number of CFs with more than 50 flashes (solid lines) divided by the total number of CFs (dotted lines) in each bin. Intense CFs have a higher probability of occurring over land than over ocean, which is consistent with previous studies (Cecil & Blankenship, 2012; Spencer & Santek, 1985; Zipser et al., 2006). The probability of intense convection remains relatively low when there is a low CAPE (<1,000 J/kg; Figure 2a). Then the probability increases rapidly with increasing CAPE until sample size (dotted lines) becomes small enough (CAPE >4,000 J/kg) that the estimates might be inaccurate. With a peak with CIN values between 120 and 200 J/kg, the probability of intense CFs associated with CIN increases with increasing CIN and then starts to decrease when the value exceeds 200 J/kg (Figure 2b). Over the ocean, the variation in the probability of intense thunderstorms associated with CIN is small. This is because the magnitude of CIN is relatively smaller over ocean than over land (Williams & Renno, 1993). Over land, high CIN could allow CAPE to build up rapidly through a suppression of entrainment under conditions of surface heating and boundary layer growth (Parker, 2002).

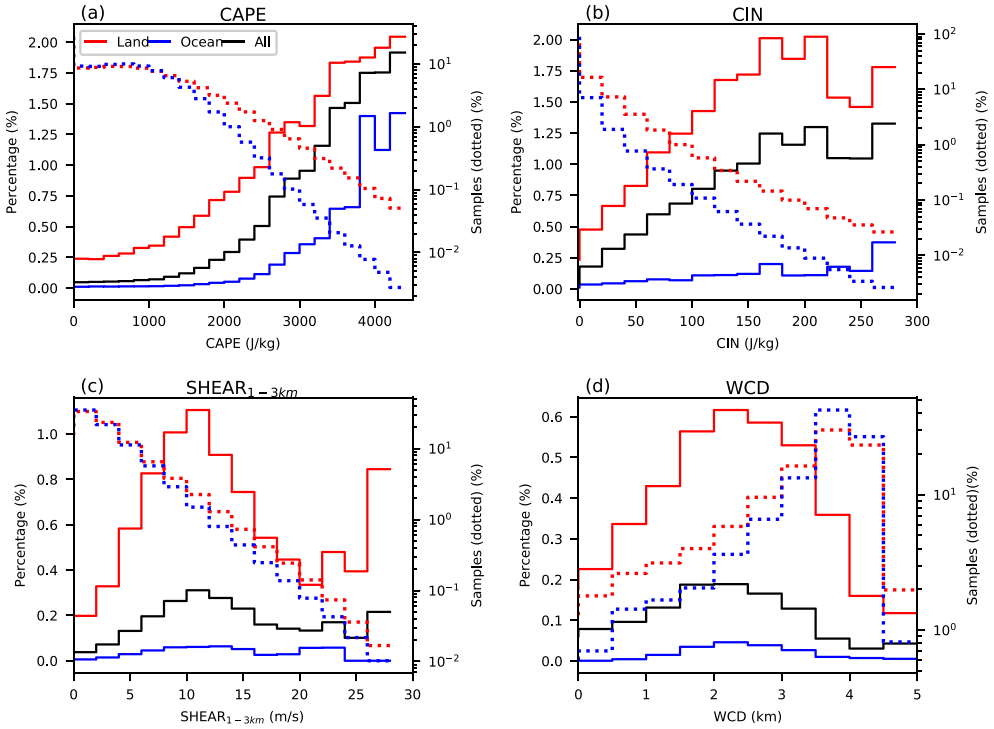

Figure 2. Percentage of CFs with more than 50 flashes versus one specific thermodynamic variable. (a) CAPE, (b) CIN, (c) $SHEAR_{1-3\ km}$, and (d) WCD. The dotted red (blue) lines indicate the total number contributing to each bin for the TRMM CFs over land (ocean). The percentage is calculated as the number of CFs with more than 50 flashes divided by the total number of CFs in each bin. The solid lines are for land (solid), ocean (blue), and all regions (black) in 36°S–36°N.

Convection tends to be more widespread but shallower over the ocean under lower CIN conditions in comparison to that over land. The probability of intense events as it relates to wind shear shows a bimodal dependence on the shear (Figure 3c), which has also been suggested in a prior study (Westermayer et al., 2016). They have explained this bimodal distribution of the probability of thunderstorms related to wind shear by a combination of two effects. First, towering cumulus clouds are not tilted and are more likely to develop into intense thunderstorms in a weak shear environment than in a strong shear one. On the other hand, strong wind shear usually occurs in the vicinity of fronts or jets, which could help initiate and maintain the well-organized systems once they form. However, moderate wind shear is detrimental to the isolated storms and is not sufficient to initiate organized convection by the frontal systems. The pattern of the probability of intense thunderstorms as a function of WCD shows a peak when WCD values are between 2 and 3 km, though most of the CFs have WCD deeper than 3.5 km.

Figure 3 shows the population of total CFs (contours) and probability of intense CFs (color fill) as a function of two environmental variables, based on CFs over the whole TRMM domain. The number of samples is sufficiently large, as shown by the gray contours. These represent the two-dimensional histogram of the population of CFs as a function of two of the four variables: CAPE, CIN, $SHEAR_{1-3\ km}$, and WCD. Environments with small CAPE (<1,000 J/kg) are not favorable for intense thunderstorms (Figure 3a). In environments with moderate CAPE (1,000–2,500 J/kg), the probability of intense CFs associated with moderate CIN (100–200 J/kg) is higher than that associated with small CIN (<50 J/kg). This implies that CIN may help accumulate the moist static energy and increase the potential for intense thunderstorms in environments with moderate CAPE. Environments with large CAPE (>3,000 J/kg) and small CIN (<100 J/kg) are also favorable for intense convection. As a widely accepted factor for identifying intense weather days, larger low-level wind shear is associated with a higher probability of intense CFs for a constant value of CAPE (Figure 3b). Under an unstable environment with CAPE >2,000 J/kg, shallower WCD is favorable for intense thunderstorms (Figure 3c). This is consistent with the results shown by Stolz et al. (2015) that the total lightning density increases with decreasing WCD. With moderate CIN (100–200 J/kg), an

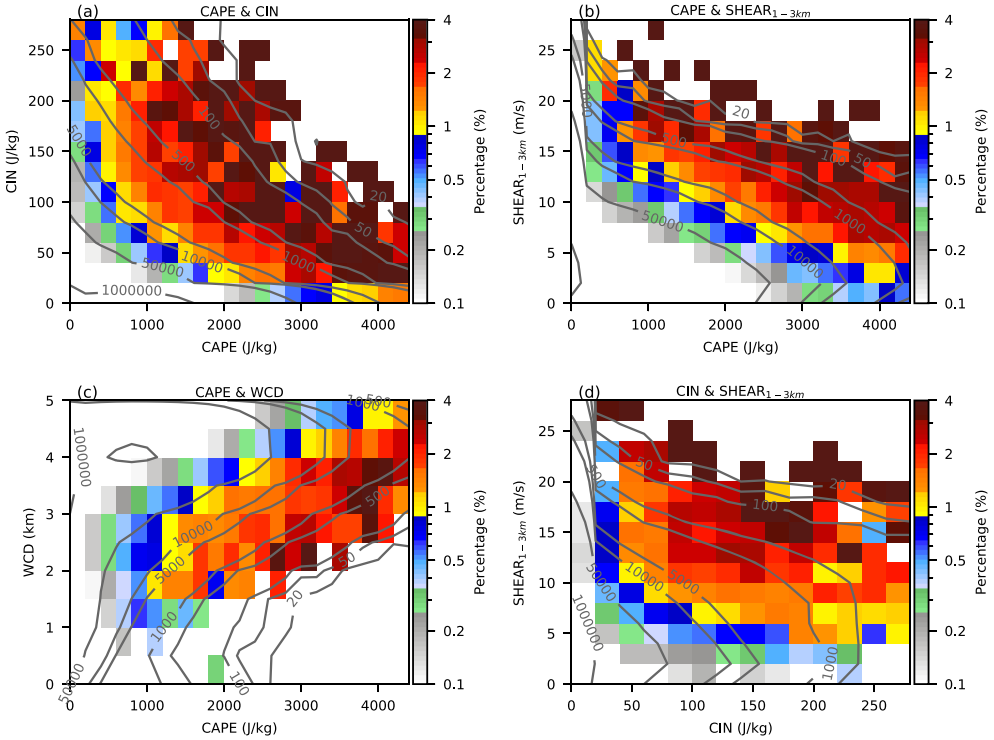

Figure 3. Percentage of CFs with more than 50 flashes versus two specific thermodynamic variables jointly. (a) CAPE and CIN, (b) CAPE and $SHEAR_{1-3\ km}$, (c) CAPE and WCD, and (d) CIN and $SHEAR_{1-3\ km}$. Contours represent the distribution of the population of CFs. The color fill shows the percentage of CFs with more than 50 flashes as a function of two variables.

environment with stronger low-level wind shear is more favorable for intense thunderstorms than an environment with weaker wind shear (Figure 3d).

3.2. Reconstruct the Probability of Intense Thunderstorms From Thermodynamic Variables

As shown in Figures 2 and 3, the relationships between the probability of intense thunderstorms and their environmental variables have major implications for understanding which environments are able to support intense thunderstorms. Therefore, the relationships computed from equation (1) are used as lookup tables to examine the regional variation of intense thunderstorms.

3.2.1. Using one thermodynamic variable

The probability of intense thunderstorms is estimated by applying the lookup tables to one environmental variable, which is derived from 6 hourly ERA-Interim reanalysis data with a 0.75° × 0.75° horizontal resolution. Note that the probability of intense CFs is conditional in Figure 2. In other words, it is the probability of intense thunderstorms under the condition that a CF occurs. Therefore, the precondition of precipitation rate greater than zero (millimeter per hour) is considered in order to apply the lookup tables. The precipitation rate is derived from the 3 hourly, 0.25° × 0.25° TRMM 3B42 (v7) precipitation products (Huffman et al., 2007). To be consistent with the resolution of ERA-Interim reanalysis data, the TRMM 3B42 data are linearly interpolated onto the same ERA-Interim 0.75° × 0.75° grid. Then, on each reanalysis grid point with precipitation greater than zero, the probability of intense thunderstorms is estimated by applying the lookup tables. To further explore the geographical distribution of intense thunderstorms, the average of the probability of intense thunderstorms is reconstructed on a 2° × 2° grid, as shown in Figures 4 and 5.

Figure 4 shows the reconstructed geographical distribution of the probability of intense thunderstorms from one environmental variable, based on the lookup table created for the whole TRMM domain without consideration of land versus ocean in Figure 2. Unsurprisingly, the performance is poor when only one environmental factor is considered to estimate the probability of intense thunderstorms. The geographical distribution in Figure 4a reveals that regions with higher probability of intense thunderstorms estimated

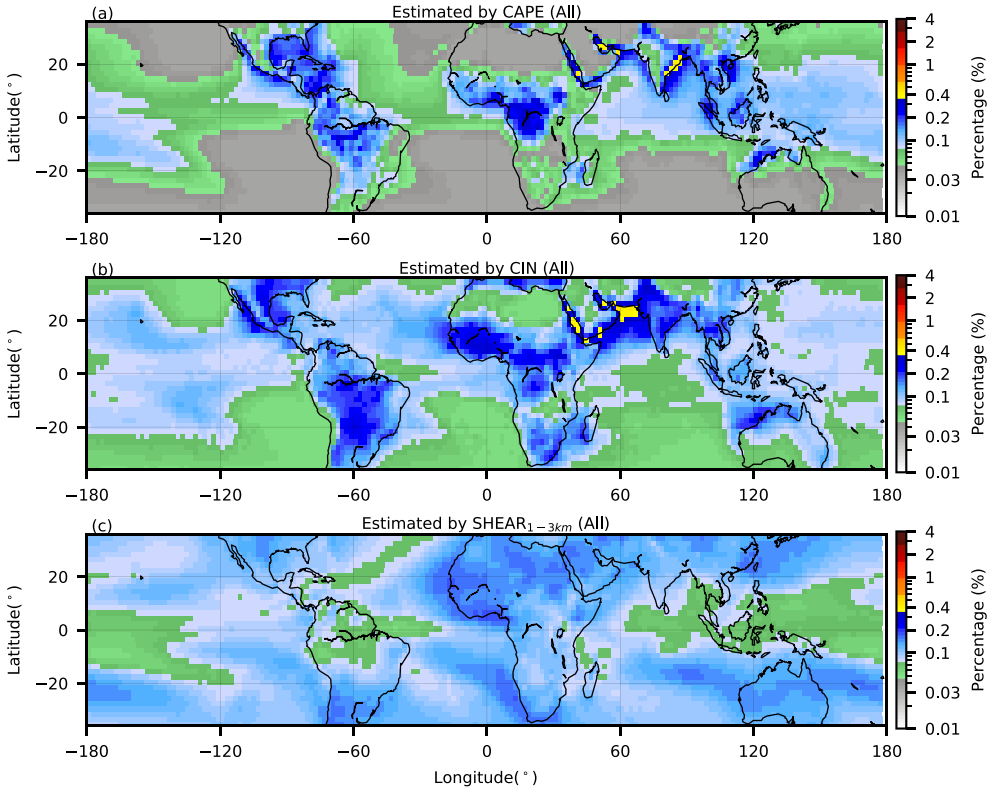

Figure 4. Estimated geographical distribution of the percentage of intense thunderstorms based on individual environmental variables. (a) CAPE, (b) CIN, and (c) $SHEAR_{1-3\ km}$. The probability of intense thunderstorms is estimated using the lookup tables shown in Figure 2. Thermodynamic variables are derived from 6 hourly ERA-Interim reanalysis data with a 0.75° × 0.75° horizontal resolution. "All" means that land and ocean are considered together when lookup tables are created.

from CAPE, such as the Gulf of Mexico, the Amazon, central Africa, and the Maritime Continents, are associated with higher potential energy. However, these regions are not favorable for intense thunderstorms as shown in Figure 1c. This implies that an atmosphere with high moist potential energy alone is insufficient for intense convection. Regions with relative high probability of intense thunderstorms estimated by CIN are found over land, especially downstream of major mountain ranges. This indicates that large topographical features may play an important role in creating CIN (e.g., Hanley et al., 2011; Peckham & Wicker, 2000; Rasmussen & Houze, 2016). Low-level wind shear alone is not capable of estimating the probability of intense thunderstorms (Figure 4c). That is why the combination of CAPE and shear is commonly used to identify the potential for intense weather (e.g., Allen et al., 2015; Diffenbaugh et al., 2013; Sander et al., 2013).

3.2.2. Using two thermodynamic variables

The percentages of intense thunderstorm as function of two thermodynamic variables in Figure 3 are used as lookup tables to estimate the probability of intense thunderstorms. There is a clear improvement in the performance of the estimation when a combination of two environmental variables is used to reconstruct the geographical distribution of intense thunderstorms (Figure 5). A combination of CAPE and CIN can reproduce the probability of intense thunderstorms over a few specific regions, such as the vicinity of the Himalayas, West Africa, and central Africa. The underestimation over West Africa and Argentina by CAPE and CIN indicates the important role of other factors, such as wind shear, in the probability of intense thunderstorms (Figure 5a). Figure 5b shows that the probability of intense thunderstorms tends to be underestimated downstream of major mountain ranges when CIN is not considered. This confirms the results shown in previous studies (e.g., Houze et al., 2007; Rasmussen & Houze, 2011; Romatschke et al., 2010) that dry warm air flowing off the mountains provides a cap; therefore, the high moist energy air has more CIN to overcome. In this case, convective instability can be stored and accumulated in the environment. Under these conditions, intense convection is more likely to develop once the accumulated instability can be

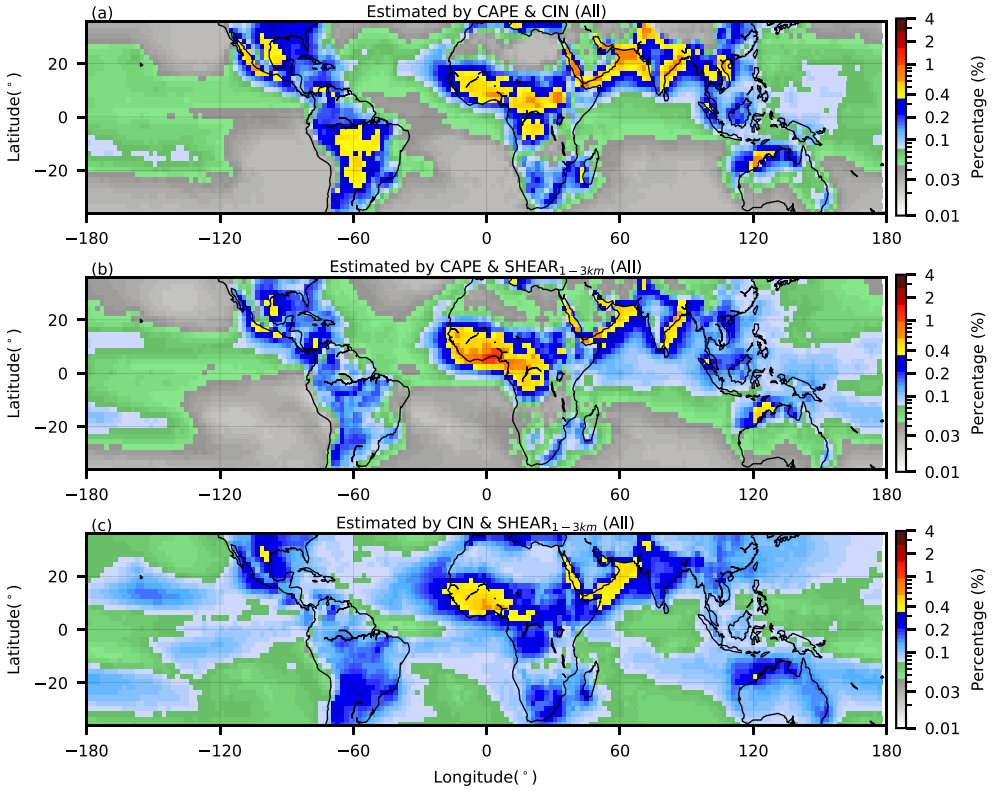

Figure 5. Same as Figure 4, but estimated with two variables. (a) CAPE and CIN, (b) CAPE and $SHEAR_{1-3\ km}$, and (c) CIN and $SHEAR_{1-3\ km}$.

released explosively. It is worth noting that the distinct difference of the probability in intense thunderstorms between land and ocean can be separated by only two environmental variables, though still overestimating over ocean.

3.2.3. Probability of intense thunderstorms using CAPE, CIN, and $SHEAR_{1-3\ km}$

Prior studies (e.g., Mapes, 1997; Raymond & Herman, 2011; Weisman & Klemp, 1986) have made efforts to estimate the occurrence of intense thunderstorms from a few environmental factors, individually and by using two variables jointly. Here, the sufficiently large number of samples from 16-year TRMM observations enables us to add more information to estimate the probability of intense thunderstorms. Using a similar approach, lookup tables using three variables have been created, and the geographical distribution of intense thunderstorms has been estimated with these lookup tables using ERA-Interim fields. The best results are obtained from the combination of CAPE, CIN, and $SHEAR_{1-3\ km}$ (Figure 6). Compared to the observations in Figure 1c, the geographical distribution of thunderstorms percentage is closely reproduced, in both magnitude and general distribution pattern. For example, Argentina, another hot spot for intense thunderstorms, starts to stand out when adding the third factor (Figure 6a). However, the occurrence is still overestimated over ocean. When lookup tables of land and ocean are used separately, the estimated probability of intense thunderstorms over ocean is close to the observations shown in Figure 1c. In addition, the combination of these three factors gives a good delineation of the favorable environment for intense thunderstorms over the southwest United States and Colombia, locations shown to be favorable for intense thunderstorms.

3.2.4. Consideration of four thermodynamic variables

Pushing the limit of the samples further, a fourth factor is added in the process of reproducing the distribution of intense thunderstorms. We tested several variables including LCL, SHL, RHM, LI_{500}, TCWV, and WCD. Here, the one with the best performance (WCD) is displayed in Figure 7. The combination of these four factors in Figure 7a captures these hot spots of intense thunderstorms with more than 50 flashes shown in Figure 1c, despite some overestimation over the Arabian Sea. When we apply the lookup table that considers the land and ocean separately, further improvement is seen over oceans, the south central United States, and Argentina.

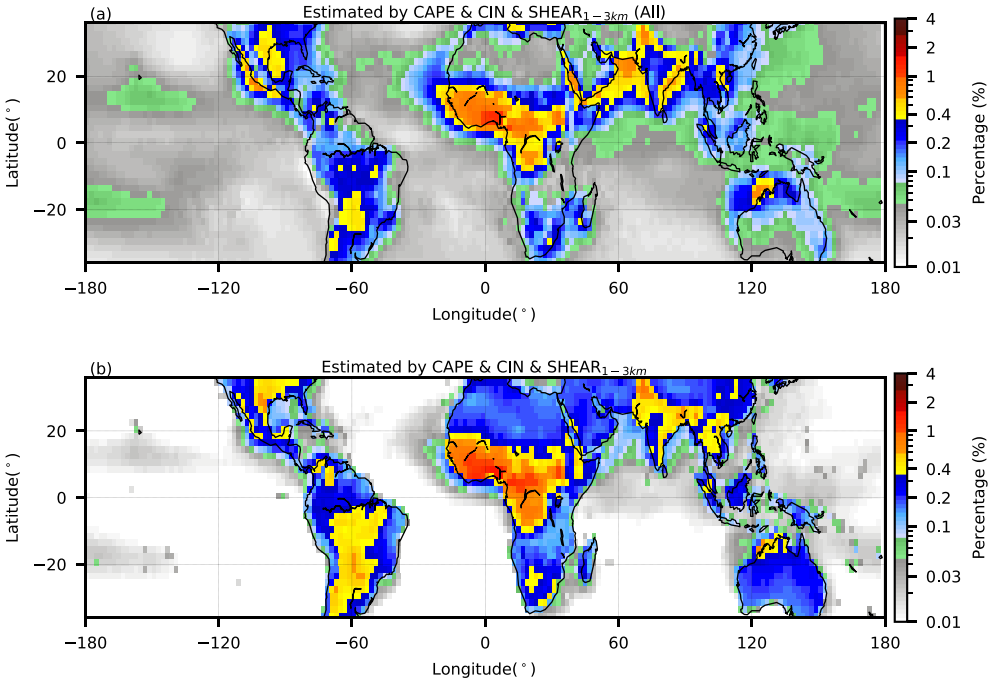

Figure 6. Same as Figures 4 and 5, but estimated with three variables: CAPE, CIN, and $SHEAR_{1-3\ km}$. (a) No separation of land and ocean. (b) Considering land and ocean separately.

Together with the combination of CAPE, CIN, and $SHEAR_{1-3\ km}$, the best performance of the fourth factor is from WCD. In this study, we use lightning flashes as a proxy to identify intense thunderstorms, which involves storm electrification. Electrification has been suggested to be associated with the mass of cloud ice particles in the appropriate temperature range of 0 °C to −40 °C in models (e.g., Baker et al., 1995;

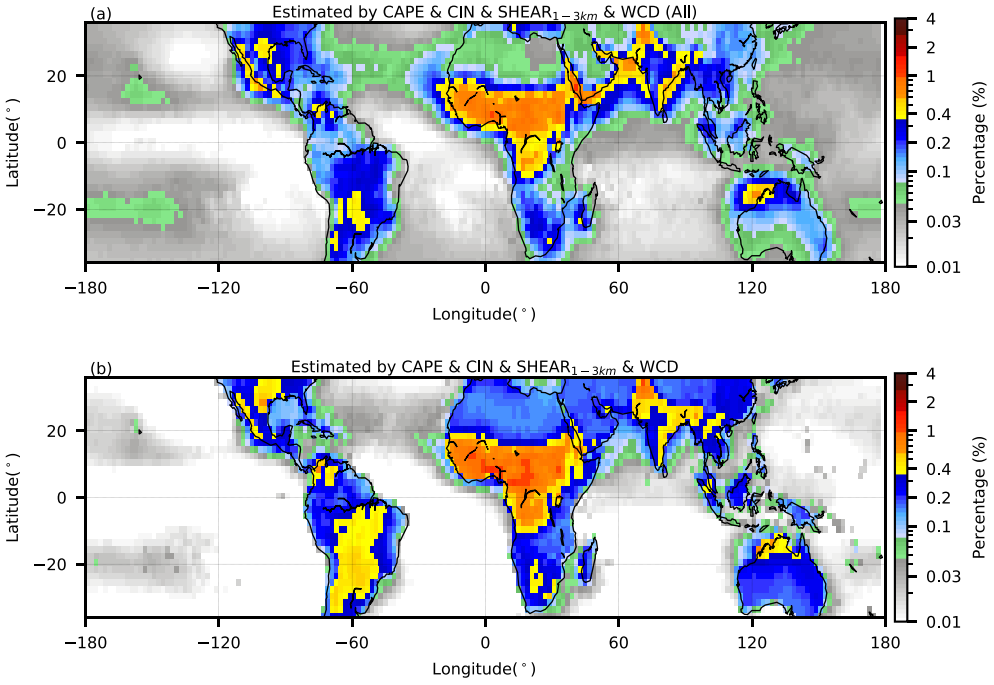

Figure 7. Same as Figures 4–6, but estimated by four variables: CAPE, CIN, $SHEAR_{1-3\ km}$, and WCD. (a) No separation of land and ocean. (b) Considering land and ocean separately.

Table 2
Mean and Spatial Correlations Between the Observed Percentage of CFs With >50 Flashes and Estimated Percentage of Intense Thunderstorms by Individual and Joint Atmospheric Factors

		Land and ocean separately				Land and ocean together			
		Land		Ocean		Land		Ocean	
Atmospheric factors		Mean	*R*	Mean	*R*	Mean	*R*	Mean	*R*
	Observations	0.53		0.10					
One	CAPE	0.26	0.38	0.03	0.29	0.09	0.29	0.07	0.25
	CIN	0.33	0.52	0.03	0.32	0.14	0.51	0.09	0.31
	$SHEAR_{1-3\ km}$	0.40	0.27	0.04	0.30	0.12	0.23	0.10	0.21
Two	CAPE + CIN	0.30	0.56	0.03	0.35	0.19	0.55	0.07	0.36
	CAPE + $SHEAR_{1-3\ km}$	0.30	0.54	0.03	0.38	0.14	0.48	0.08	0.35
	CIN + $SHEAR_{1-3\ km}$	0.37	0.63	0.04	0.38	0.17	0.64	0.10	0.40
Three	CAPE + CIN + $SHEAR_{1-3\ km}$	0.31	0.59	0.03	0.41	0.21	0.59	0.07	0.41
Four	CAPE + CIN + $SHEAR_{1-3\ km}$ + TCWV	0.39	0.61	0.06	0.44	0.29	0.60	0.10	0.42
	CAPE + CIN + $SHEAR_{1-3\ km}$ + LCL	0.47	0.63	0.06	0.43	0.41	0.62	0.09	0.44
	CAPE + CIN + $SHEAR_{1-3\ km}$ + SHL	0.42	0.63	0.07	0.53	0.31	0.64	0.09	0.54
	CAPE + CIN + $SHEAR_{1-3\ km}$ + RHM	0.45	0.63	0.07	0.45	0.34	0.61	0.11	0.44
	CAPE + CIN + $SHEAR_{1-3\ km}$ + LI500	0.66	0.50	0.07	0.33	0.51	0.49	0.16	0.36
	CAPE + CIN + $SHEAR_{1-3\ km}$ + WCD	0.41	0.66	0.06	0.53	0.30	0.65	0.08	0.53

Sherwood et al., 2006). WCD, the difference between the LCL and the freezing height, is directly related to the warm rain process and amount of water being lifted to the mixed-phase levels; this could be one of the reasons why WCD is helpful in the estimation of thunderstorms with more lightning flashes.

In summary, Table 2 lists the mean and spatial correlations between the observed percentage of CFs with more than 50 flashes and the estimated percentage of intense thunderstorms by individual and joint thermodynamic variables. The difference in the spatial correlations between the observed and estimated probability of intense thunderstorms tends to decrease when more factors are considered. Moreover, better performance is found when land and ocean are considered separately than when considering land and ocean together. This implies that factors considered cannot fully represent the contrast in the environmental conditions over land and ocean. When more factors are considered, the differences in the performance between the two types of lookup tables become smaller, suggesting that the combination of more factors can capture more of the physical processes for the land versus ocean contrast. The best performance is from the combination of CAPE, CIN, $SHEAR_{1-3\ km}$, and WCD, which is reflected in the highest spatial correlation between the observed and estimated probability of intense thunderstorms. The second highest spatial correlation between the observation and the estimation is associated with the first three and SHL. This indicates that the low-level moisture, which has been emphasized in modeling contexts (e.g., Droegemeier & Wilhelmson, 1985; Reap & MacGorman, 1989; Yano et al., 2013), is another important factor in the estimation of intense thunderstorms. The relatively high spatial correlations for LCL and RHM suggest that they are also useful in the prediction of intense thunderstorms. TCWV, a useful predictor for large precipitating systems (Chen et al., 2017), with the combination of CAPE, CIN, and $SHEAR_{1-3\ km}$, does not show good performance in the estimation of intense thunderstorms with high-flash rate. The spatial correlation related to LI_{500} is relatively low, compared to other variables. One reason for this is because instability information has already been included in the analysis by using CAPE. Although both LI_{500} and CAPE have been used as measures of instability, CAPE often provides a better overall profile of instability than LI_{500}, which uses a single atmospheric layer.

3.3. The Seasonal Variation of Intense Thunderstorms Over Selected Regions

Because the relationship between intense thunderstorms and large-scale environments could vary in different seasons, efforts are made here to determine the seasonal variation of intense thunderstorms from the four thermodynamic variables and their correlation with the observations over selected regions (Figure 8). These regions include Argentina (ARGEN), Himalaya (HIMA), West Africa (WAFRICA), central Africa (CAFRICA), and the south central United States (SCUS; boxes shown in Figure 1c). The seasonal variation of intense thunderstorms over ARGEN is smaller than that over the other selected regions. Over CAFRICA,

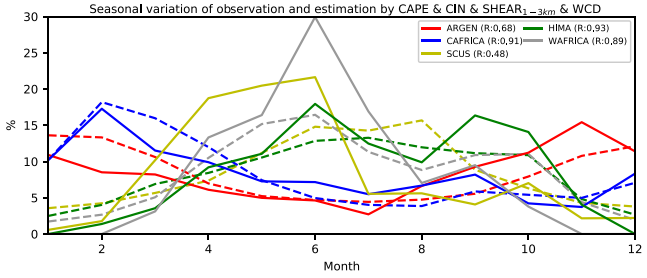

Figure 8. Seasonal variations of the observed (solid lines) and estimated (dashed lines) percentages of intense thunderstorms over selected regions (as shown in Figure 1c): ARGEN, HIMA, WAFRICA, CAFRICA, and SCUS. The correlations between the observed and estimated percentages of intense thunderstorms over different regions are shown in the legend. The estimated seasonal variations are created based on the four atmospheric variables: CAPE, CIN, $SHEAR_{1-3\ km}$, and WCD.

the reconstructed seasonal variation is in agreement with the observations. With two peaks in spring and fall, the estimated seasonal variation of intense thunderstorms is consistent with the observation over HIMA and WAFRICA. The underestimation (overestimation) of the second peak in September for HIMA (WAFRICA) confirms that the favorable environment for intense thunderstorms varies in different seasons, even in the same region. Over SCUS, more than 40% of thunderstorms during April, May, and June are found to be associated with drylines (e.g., Peterson, 1983; Rhea, 1966; Schaefer, 1974), boundaries between moist air from the Gulf of Mexico and dry air from arid regions in northern Mexico, eastern New Mexico, and western Texas. However, none of the variables used here are good representative parameters for these boundaries. This might be one of the reasons that the peak of intense thunderstorms is found in summer (June, July, and August) by thermodynamic variables while the observed peak of intense thunderstorms occurs in spring and early summer (April, May, and June).

4. Discussion

Caution must be taken in interpreting the results here. First, the ERA-Interim reanalysis data have uncertainties resulting from the forecast model, data assimilation, and data sources used (Courtier et al., 1994; Dee et al., 2011; Uppala et al., 2008). The calculation of CAPE is still open to debate because of the various assumptions about the parcel level of origin, characteristics of parcel moisture and temperature, ascent path, and the presence or absence of the ice phase (Craven et al., 2002; Doswell & Rasmussen, 1994; Emanuel, 1994; Williams & Renno, 1993). Also, it is known that the potential energy would be released almost instantaneously once it is triggered by sufficient lifting, such as synoptic ascent, low-level convergence, and orographic lifting (e.g.,Berry & Thorncroft, 2005 ; Houze et al., 2007 ; Mekonnen et al., 2006 ; Rasmussen & Houze, 2016). Second, here we have discussed the convective precipitation with high lightning rates, which involves electrification processes. Though we refer these samples as convectively intense, the relationships to thermodynamic variables might vary for intense convective clouds if differently identified, such as by intense radar echoes at high altitudes. Consideration should be given in the application to different types of systems. For example, TCWV has been suggested to be strongly associated with the large-size precipitation systems (Zhou et al., 2013; Chen et al., 2017). Third, the effects of aerosol in the estimation of thunderstorms are not considered in this study because of the considerable uncertainty of their role in deep convection and lightning (e.g., Koren et al., 2012; Lee, 2012; Wall et al., 2014; Williams & Stanfill, 2002). In addition, even if the environment is favorable for an intense thunderstorm, it does not mean one would occur. For example, here we have not discussed the mechanism of initiation of convection. Even with these limitations, the investigation in this study demonstrates that it is possible to utilize the satellite observed historical events and reanalysis data to understand the relationships between large-scale environments and subgrid scale convective processes. The approach used here can be developed further to parameterize proxies for thunderstorms in climate models, reanalysis, and numerical weather prediction models.

5. Summary

The analysis of a 16-year TRMM CFs data set has shown that the probability of high-flash rate thunderstorms is related to their thermodynamic and kinematic environmental variables. Those environmental variables, derived from the ERA-Interim reanalysis data, include CAPE, CIN, $SHEAR_{1-3\ km}$, WCD, LCL, TCWV, SHL, RHM, and LI_{500}. Each corresponds to certain physical processes. In order to examine the relationships between thermodynamic environments and the occurrence of high-flash rate thunderstorms, Bayesian-like models are built on the probability of intense CFs and their collocated ERA-Interim environmental variables.

Two types of lookup tables have been built based on the relationship between the probability of those events and the environmental conditions. One considers the whole TRMM domain including both land and ocean, while the other considers land and ocean separately. Then, those lookup tables have been used to reconstruct the geographical distribution of high-flash rate thunderstorms across the tropics and subtropics.

The relationships between single, as well as a combination of two or more environmental variables, and the probability of high-flash rate thunderstorms are examined. It is shown that any single thermodynamic or kinematic variable alone cannot fully represent the global geographical distribution of high-flash rate thunderstorms. The general pattern of the geographical distribution derived from a combination of the four variables CAPE, CIN, $SHEAR_{1-3\ km}$, and WCD agrees well with the TRMM observations. The estimated seasonal variation of high-flash rate events from these four variables over various selected regions captures the two peaks in the seasonal variation of high-flash rate thunderstorms occurring in June and September over HIMA and WAFRICA and small variations over CAFRICA and ARGEN.

All these results suggest that the high-flash rate thunderstorms, mainly found in certain regions and seasons, can be largely interpreted by the specific combinations of favorable thermodynamic and kinematic environments. While this study focuses on high-flash rate thunderstorms, we speculate that similar results would have resulted if intense thunderstorms had been defined by other intensity proxies, such as the minimum PCT at 85 and 37 GHz and maximum 40-dBZ echo top heights.

Acknowledgments
Thanks to Douglas C. Stolz, Toshi Matsui, and an anonymous reviewer for their valuable comments and suggestions. This research was supported by NASA Precipitation Measurement Mission Grants 80NSSC19K0673 under the direction of Dr. Gail Skofronick-Jackson and NNX16AH74G under the direction of Dr. Erich Stocker. Thanks to the Precipitation Processing System (PPS) team at NASA Goddard Space Flight Center, Greenbelt, MD, for data processing assistance. The authors thank Lindsey Hayden for English editing. These TRMM data can be downloaded online (http://atmos.tamucc.edu/trmm/data/). The ERA-Interim data are obtained online (https://apps.ecmwf.int/datasets/data/interim-full-daily).

References

Albrecht, R., Goodman, S. J., Petersen, W. A., Buechler, D. E., Bruning, E. C., Blakeslee, R. J., & Christian, H. J. (2011). *The 13 years of TRMM Lightning Imaging Sensor: From individual flash characteristics to decadal tendencies, paper presented at* XIV International Conference on Atmospheric Electricity, Int. Comm. on Atmos. Electr. Rio de Janeiro, Brazil.

Albrecht, R. I., Goodman, S. J., Buechler, D. E., Blakeslee, R. J., & Christian, H. J. (2016). Where are the lightning hotspots on Earth? *Bulletin of the American Meteorological Society*, *97*, 2051–2068. https://doi.org/10.1175/BAMS-D-14-00193.1

Allen, J. T., Tippett, M. K., & Sobel, A. H. (2015). An empirical model relating U.S. monthly hail occurrence to large-scale meteorological environment. *Journal of Advances in Modeling Earth Systems*, *7*, 226–243. https://doi.org/10.1002/2014MS000397

Anquetin, S., Yates, E., Ducrocq, V., Samouillan, S., Chancibault, K., Davolio, S., et al. (2005). The 8 and 9 September 2002 flash flood event in France: A model intercomparison. *Natural Hazards and Earth System Sciences*, *5*, 741–754.

Baker, M. B., Christian, H. J., & Latham, J. (1995). A computational study of the relationships linking lightning frequency and other thundercloud parameters. *Quarterly Journal of the Royal Meteorological Society*, *121*, 1525–1548.

Bennett, L. J., Browning, K. A., Blyth, A. M., Parker, D. J., & Clark, P. A. (2006). A review of the initiation of precipitating convection in the United Kingdom. *Quarterly Journal of the Royal Meteorological Society*, *132*, 1001–1020.

Berry, G. J., & Thorncroft, C. (2005). Case study of an intense African easterly wave. *Monthly Weather Review*, *133*, 752–766. https://doi.org/10.1175/MWR2884.1

Blanchard, D. (1998). Assessing the vertical distribution of CAPE. *Weather and Forecasting*, *13*, 870–877.

Brooks, H. E., Lee, J. W., & Craven, J. P. (2003). The spatial distribution of intense thunderstorm and tornado environments from global reanalysis data. *Atmospheric Research*, *67–68* 73–94.

Brown, B. G., & Murphy, A. H. (1996. Verification of aircraft icing forecasts: The use of standard measures and meteorological covariates. Preprints, 13th Conf. on Probability and Statistics in the Atmospheric Sciences, San Francisco, CA, Amer. Meteor. Soc., 251–252.

Carey, L. D., Petersen, W. A., & Rutledge, S. A. (2003). Evolution of cloud-to-ground lightning and storm structure in the Spencer, South Dakota, tornadic supercell of 30 May 1998. *Monthly Weather Review*, *131*, 1811–1831. https://doi.org/10.1175//2566.1

Cecil, D. J., & Blankenship, C. B. (2012). Toward a global climatology of intense hailstorms as estimated by satellite passive microwave imagers. *Journal of Climate*, *25*, 687–703.

Cecil, D. J., Buechler, D. E., & Blakeslee, R. J. (2014). Gridded lightning climatology from TRMM-LIS and OTD: Dataset description. *Atmospheric Research*, *135–136*, 404–414.

Chen, B., Liu, C., & Mapes, B. E. (2017). Relationships between large precipitating systems and atmospheric factors at a grid scale. *Journal of the Atmospheric Sciences*, *74*, 531–552.

Courtier, P., Thépaut, J. N., & Hollingsworth, A. (1994). A strategy for operational implementation of 4D-Var, using an incremental approach. *Quarterly Journal of the Royal Meteorological Society*, *120*, 1367–1387.

Craven, J., Jewell, R., & Brook, H. (2002). Comparison between observed convective cloud-base heights and lifting condensation level for two different lifted parcels. *Weather and Forecasting*, *17*, 885–890.

Davies, J. M. (2004). Estimations of CIN and LFC associated with tornadic and non-tornadic supercells. *Weather and Forecasting*, *19*, 714–726.

Dee, D. P., Uppala, S. M., Simmons, A. J., Berrisford, P., Poli, P., Kobayashi, S., et al. (2011). The ERA-Interim reanalysis: Configuration and performance of the data assimilation system. *Quarterly Journal of the Royal Meteorological Society*, *137*(656), 553–597. https://doi.org/10.1002/qj.828

Diffenbaugh, N. S., Scherer, M., & Trapp, R. J. (2013). Robust increases in intense thunderstorm environments in response to greenhouse forcing. *Proceedings of the National Academy of Sciences of the United States of America*, *110*, 16,361–16,366. https://doi.org/10.1073/pnas.1307758110

Doswell, C. A. III, & Evans, J. S. (2003). Proximity sounding analysis for derechos and supercells: An assessment of similarities and differences. *Atmospheric Research*, *67–68*, 117–133.

Doswell, C. A. III, & Rasmussen, E. N. (1994). The effect of neglecting the virtual temperature correction on CAPE calculations. *Weather and Forecasting*, *9*, 625–629.

Droegemeier, K. K., & Wilhelmson, R. B. (1985). Three-dimensional numerical modeling of convection produced by interacting thunderstorm outflows. Part I: Control simulation and low-level moisture variations. *Journal of the Atmospheric Sciences*, *42*, 2381–2403.

Emanuel, K. A. (1994). *Atmospheric convection*. New York: Oxford University Press.

Feng, Z., Leung, L. R., Hagos, S., Houze, R. A., Burleyson, C. D., & Balaguru, K. (2016). More frequent intense and long-lived storms dominate the springtime trend in central US rainfall. *Nature Communications*, *7*, 13429.

Foote, G. B., & Mohr, C. G. (1979). Results of a randomized hail suppression experiment in northeast Colorado. Part VI: Post hoc stratification by storm type and intensity. *Journal of Applied Meteorology*, *18*, 1589–1600.
Gallus, W. A., Correia, J., & Jankov, I. (2005). The 4 June 1999 derecho event: A particularly difficult challenge for numerical weather prediction. *Weather and Forecasting*, *20*, 705–728.
Galway, J. G. (1956). The lifted index as a predictor of latent instability. *Bulletin of the American Meteorological Society*, *37*, 528–529. https://doi.org/10.1175/1520-0477-37.10.528
Hanley, K. E., Kirshbaum, D. J., Belcher, S. E., Roberts, N. M., & Leoncini, G. (2011). Ensemble predictability of an isolated mountain thunderstorm in a high-resolution model. *Quarterly Journal of the Royal Meteorological Society*, *137*, 2124–2137.
Holloway, C. E., & Neelin, J. D. (2009). Moisture vertical structure, column water vapor, and tropical deep convection. *Journal of the Atmospheric Sciences*, *66*, 1665–1683.
Houze, R. A. (1993). *Cloud dynamics*, (p. 573). Academic Press.
Houze, R. A. Jr., Rasmussen, K. L., Zuluaga, M. D., & Brodzik, S. R. (2015). The variable nature of convection in the tropics and subtropics: A legacy of 16 years of the Tropical Rainfall Measuring Mission satellite. *Reviews of Geophysics*, *53*, 994–1021. https://doi.org/10.1002/2015RG000488
Houze, R. A., Wilton, D. C., & Smull, B. F. (2007). Monsoon convection in the Himalayan region as seen by the TRMM Precipitation Radar. *Quarterly Journal of the Royal Meteorological Society*, *133*, 1389–1411. https://doi.org/10.1002/qj.106
Huffman, G. J., Bolvin, D. T., Nelkin, E. J., Wolff, D. B., Adler, R. F., Gu, G., et al. (2007). The TRMM Multisatellite Precipitation Analysis (TMPA): Quasi-global, multiyear, combined-sensor precipitation estimates at fine scales. *Journal of Hydrometeorology*, *8*, 38–55.
Kain, J. S., Coniglio, M. C., Correia, J., Clark, A. J., Marsh, P. T., Ziegler, C. L., et al. (2013). A feasibility study for probabilistic convection initiation forecasts based on explicit numerical guidance. *Bulletin of the American Meteorological Society*, *94*, 1213–1225. https://doi.org/10.1175/BAMS-D-11-00264.1
Kaltenböck, R., Diendofer, G., & Dotzek, N. (2009). Evaluation of thunderstorm indices from ECMWF analyses, lightning data and intense storms reports. *Atmospheric Research*, *93*, 381–396.
Koren, I., Altaratz, O., Remer, L. A., Feingold, G., Vanderlei Martins, J., & Heiblum, R. H. (2012). Aerosol-induced intensification of rain from the tropics to the midlatitudes. *Nature Geoscience*, *5*, 118–122. https://doi.org/10.1038/ngeo1364
Kummerow, C., Barnes, W., Kozu, T., Shiue, J., & Simpson, J. (1998). The Tropical Rainfall Measuring Mission (TRMM) sensor package. *Journal of Atmospheric and Oceanic Technology*, *15*, 809–817.
Lang, T. J., & Rutledge, S. A. (2002). Relationships between convective storm kinematics, precipitation, and lightning. *Monthly Weather Review*, *130*, 2492–2506.
Lee, S. S. (2012). Effect of aerosol on circulations and precipitation in deep convective clouds. *Journal of the Atmospheric Sciences*, *69*, 1957–1974. https://doi.org/10.1175/JAS-D-11-0111.1
Liu, C., & Zipser, E. (2005). Global distribution of convection penetrating the tropical tropopause. *Journal of Geophysical Research*, *110*, D23210. https://doi.org/10.1029/2005JD00006063
Liu, C., Zipser, E. J., Cecil, D. J., Nesbitt, S. W., & Sherwood, S. (2008). A cloud and precipitation feature database from nine years of TRMM observations. *Journal of Applied Meteorology and Climatology*, *47*, 2712–2728. https://doi.org/10.1175/2008JAMC1890.1
Liu, N., & Liu, C. (2016). Global distribution of deep convection reaching tropopause in 1 year GPM observations. *Journal of Geophysical Research: Atmospheres*, *121*, 3824–3842. https://doi.org/10.1002/2015JD024430
MacGorman, D. R., & Burgess, D. W. (1994). Positive cloud-to-ground lightning in tornadic storms and hailstorms. *Monthly Weather Review*, *122*, 1671–1697.
MacGorman, D. R., & Rust, W. D. (1998). *The electrical nature of storms* (p. 422). New York: Oxford University Press.
Manzato, A. (2012). Hail in northeast Italy: Climatology and bivariate analysis with the sounding-derived indices. *Journal of Applied Meteorology and Climatology*, *51*, 449–467. https://doi.org/10.1175/JAMC-D-10-05012.1
Mapes, B. (1998). The large-scale part of tropical mesoscale convective system circulations. *Journal of the Meteorological Society of Japan Series II*, *76*, 29–55.
Mapes, B. E. (1997). Equilibrium vs. activation control of large-scale variations of tropical deep convection. In R. K. Smith (Ed.), *The Physics and Parameterization of Moist Atmospheric Convection*, (pp. 321–358). Kluwer Academic.
Matsui, T., Chern, J., Tao, W.-K., Lang, S., Satoh, M., Hashino, T., & Kubota, T. (2016). On the land-ocean contrast of tropical convection and microphysics statistics derived from TRMM satellite signals and global storm-resolving models, *Journal of Hydrometeorology*, *17*, 1425–1445.
McCarthy, J. (1974). Field verification of the relationship between entrainment rate and cumulus cloud diameter. *Journal of the Atmospheric Sciences*, *31*, 1028–1039.
Mecikalski, J. R., Williams, J. K., Jewett, C. P., Ahijevych, D., LeRoy, A., & Walker, J. R. (2015). Probabilistic 0–1-h convective initiation nowcasts that combine geostationary satellite observations and numerical weather prediction model data. *Journal of Applied Meteorology and Climatology*, *54*, 1039–1059.
Meißner, C., Kalthoff, N., Kunz, M., & Adrian, G. (2007). Initiation of shallow convection in the Black Forest mountains. *Atmospheric Research*, *86*, 42–60.
Mekonnen, A., Thorncroft, C. D., & Aiyyer, A. R. (2006). Analysis of convection and its association with African easterly waves. *Journal of Climate*, *19*, 5405–5421. https://doi.org/10.1175/JCLI3920.1
Mohr, K. I., & Zipser, E. J. (1996). Defining mesoscale convective systems by their ice scattering signature. *Bulletin of the American Meteorological Society*, *77*, 1179–1189.
Moncrieff, M. W., & Miller, M. (1976). The dynamics and simulation of tropical cumulonimbus and squall lines. *Quarterly Journal of the Royal Meteorological Society*, *102*, 373–394.
Murphy, A. H. (1977). The value of climatological, categorical and probabilistic forecasts in the cost–loss ratio situation. *Monthly Weather Review*, *105*, 803–816.
Parker, D. J. (2002). The response of CAPE and CIN to tropospheric thermal variations. *Quarterly Journal of the Royal Meteorological Society*, *128*, 119–130.
Peckham, S. E., & Wicker, L. J. (2000). The influence of topography and lower-tropospheric winds on dryline morphology. *Monthly Weather Review*, *128*, 2165–2189.
Peterson, R. E. (1983). The west Texas dryline: Occurrence and behavior. Preprints, 13th Conf. Intense Local Storms, Tulsa, OK, Amer. Meteor. Soc., J9–J11.
Pierce, E. T. (1958). Some topics in atmospheric electricity. Recent Advances in Atmospheric Electricity, Pergamon, 5–16.

Rasmussen, E. N., & Blanchard, D. O. (1998). A baseline climatology of sounding-derived supercell and tornado forecast parameters. *Weather and Forecasting*, *13*, 1148–1164.
Rasmussen, K. L., & Houze, R. A. (2011). Orogenic convection in subtropical South America as seen by the TRMM satellite. *Monthly Weather Review*, *139*, 2399–2420. https://doi.org/10.1175/MWR-D-10-05006.1
Rasmussen, K. L., & Houze, R. A. (2016). Convective initiation near the Andes in subtropical South America. *Monthly Weather Review*, *144*, 2351–2374.
Raymond, D. J., & Herman, M. J. (2011). Convective quasi-equilibrium reconsidered. *Journal of Advances in Modeling Earth Systems*, *3*, M08003. https://doi.org/10.1029/2011MS000079
Reap, R. M., & MacGorman, D. R. (1989). Cloud-to-ground lightning: Climatological characteristics and relationships to model fields, radar observations, and intense local storms. *Monthly Weather Review*, *117*, 518–535.
Rhea, J. O. (1966). A study of thunderstorm formation along dry lines. *Journal of Applied Meteorology*, *5*, 58–63.
Romatschke, U., Medina, S., & Houze, R. A. (2010). Regional, seasonal, and diurnal variations of extreme convection in the South Asian region. *Journal of Climate*, *23*. https://doi.org/10.1175/2009JCLI3140.1
Romero, R., Ramis, C., & Homar, V. (2015). On the intense convective storm of 29 October 2013 in the Balearic Islands: Observational and numerical study. *Quarterly Journal of the Royal Meteorological Society*, *141*, 1208–1222. https://doi.org/10.1002/qj.2429
Rosenfeld, D., & Woodley, W. L. (2003). Closing the 50-year circle: From cloud seeding to space and back to climate change through precipitation physics. Cloud Systems, Hurricanes, and the Tropical Rainfall Measuring Mission (TRMM), Meteor. Monogr., No. 51. *American Meteorological Society*, *59–80*.
Rotunno, R., Klemp, J. B., & Weisman, M. L. (1988). A theory for strong, long-lived squall lines. *Journal of the Atmospheric Sciences*, *45*, 463–485.
Sander, J., Eichner, J. F., Faust, E., & Steuer, M. (2013). Rising variability in thunderstorm-related U.S. losses as a reflection of changes in large-scale thunderstorm forcing. *Weather, Climate, and Society*, *5*, 317–331. https://doi.org/10.1175/WCAS-D-12-00023.1
Schaefer, J. T. (1974). The life cycle of the dryline. *Journal of Applied Meteorology*, *13*, 444–449.
Schiro, K. A., Neelin, J. D., Adams, D. K., & Lintner, B. R. (2016). Deep convection and column water vapor over tropical land versus tropical ocean: A comparison between the Amazon and the tropical western Pacific. *Journal of the Atmospheric Sciences*, *73*, 4043–4063.
Sherwood, S. C., Phillips, V. T. J., & Wettlaufer, J. S. (2006). Small ice crystals and the climatology of lightning. *Geophysical Research Letters*, *33*, L05804. https://doi.org/10.1029/2005GL025242
Sherwood, S. C., Roca, R., Weckwerth, T. M., & Andronova, N. G. (2010). Tropospheric water vapor, convection, and climate. *Reviews of Geophysics*, *48*, RG2001. https://doi.org/10.1029/2009RG000301
Spencer, R. W., & Santek, D. A. (1985). Measuring the global distribution of intense convection over land with passive microwave radiometery. *Journal of Applied Meteorology*, *24*, 860–864.
Stensrud, D. J. (2007). *Parameterization schemes: Keys to understanding numerical weather prediction models* (p. 459). Cambridge, UK: Cambridge University Press.
Stolz, D. C., Rutledge, S. A., & Pierce, J. R. (2015). Simultaneous influences of thermodynamics and aerosols on deep convection and lightning in the tropics. *Journal of Geophysical Research: Atmospheres*, *120*, 6207–6231.
Stolz, D. C., Rutledge, S. A., Pierce, J. R., & van den Heever, S. C. (2017). A global lightning parameterization based on statistical relationships among environmental factors, aerosols, and convective clouds in the TRMM climatology. *Journal of Geophysical Research: Atmospheres*, *122*, 7461–7492.
Takahashi, T. (1978). Riming electrification as a charge generation mechanism in thunderstorms. *Journal of the Atmospheric Sciences*, *35*, 1536–1548.
Tompkins, A. M., & Semie, A. G. (2017). Organization of tropical convection in low vertical wind shears: Role of updraft entrainment. *Journal of Advances in Modeling Earth Systems*, *9*, 1046–1068.
Uppala, S. M., Dee, D., Kobayashi, S., & Simmons, A. (2008). Evolution of reanalysis at ECMWF. Extended Abstracts, Third WCRP Int. Conf. on Reanalysis, Tokyo, Japan, University of Tokyo, 6 pp.
Virts, K. S., Wallace, J. M., Hutchins, M. L., & Holzworth, R. H. (2013). Highlights of a new ground-based, hourly global lightning climatology. *Bulletin of the American Meteorological Society*, *94*, 1381–1391.
Wall, C., Zipser, E. J., & Liu, C. (2014). An investigation of the aerosol indirect effect on convective intensity using satellite observations. *Journal of the Atmospheric Sciences*, *71*, 430–447.
Washington, W. M., & Parkinson, C. L. (2005). An introduction to three-dimensional climate modeling, Univ. Science Books, Sausalito, Calif.
Weisman, M. L., & Klemp, J. B. (1986). Characteristics of isolated convective storms. In P. S. Ray (Ed.), *Mesoscale Meteorology and Forecasting*, (pp. 331–358). Amer. Meteor. Soc.
Weisman, M. L., & Rotunno, R. (2004). "A theory for strong long-lived squall lines" revisited. *Journal of the Atmospheric Sciences*, *61*, 361–382.
Westermayer, A. T., Groenemeijer, P., Pistotnik, G., Sausen, R., & Faust, E. (2016). Identification of favorable environments for thunderstorms in reanalysis data. *Meteorologische Zeitschrift*, *26*, 59–70. https://doi.org/10.1127/metz/2016/0754
Williams, E., & Renno, N. (1993). An analysis of the conditional stability of the tropical atmosphere. *Monthly Weather Review*, *121*, 21–36.
Williams, E. R., Geotis, S. G., Renno, N., Rutledge, S. A., Rasmussen, E., & Rickenbach, T. (1992). A Radar and Electrical Study of Tropical "Hot Towers". *Journal of the Atmospheric Sciences*, *49*, 1386–1395.
Williams, E. R., Mushtak, T. V., Rosenfeld, D., Goodman, S., & Boccippio, D. (2005). Thermodynamic conditions favorable to superlative thunderstorm updraft, mixed phase microphysics and lightning flash rate. *Atmospheric Research*, *76*, 288–306.
Williams, E. R., & Stanfill, S. (2002). The physical origin of the land–ocean contrast in lightning activity. *Comptes Rendus Physique*, *3*, 1277–1292.
Wilson, J. W., Crook, N. A., Mueller, C. K., Sun, J., & Dixon, M. (1998). Nowcasting thunderstorms: A status report. *Bulletin of the American Meteorological Society*, *79*, 2079–2099.
Wissmeier, U., & Goler, R. (2009). A comparison of tropical and midlatitude thunderstorm evolution in response to wind shear. *Journal of the Atmospheric Sciences*, *66*, 2385–2401.
Wu, X., Qie, X., Yuan, T., & Li, J. (2016). Meteorological Regimes of the Most Intense Convective Systems along the Southern Himalayan Front. *Journal of Climate*, *29*, 4383–4398.
Xia, R., Zhang, D., Zhang, C., & Wang, Y. (2018). Synoptic control of convective rainfall rates and cloud-to-ground lightning frequencies in warm-season mesoscale convective systems over North China. *Monthly Weather Review*, *146*, 813–831. https://doi.org/10.1175/MWR-D-17-0172.1

Yano, J.-I., Bister, M., Fuchs, V., Gerard, L., Phillips, V. T. J., Barkidija, S., & Piriou, J. M. (2013). Phenomenology of convection-parameterization closure. *Atmospheric Chemistry and Physics*, *13*, 4111–4131.

Ye, B., Del Genio, A. D., & Lo, K. K. (1998). CAPE variations in the current climate and in a climate change. *Journal of Climate*, *11*, 1997–2015.

Zhou, Y., Lau, W. K. M., & Liu, C. (2013). Rain characteristics and large-scale environments of precipitation objects with extreme rain volumes from TRMM observations. *Journal of Geophysical Research: Atmospheres*, *118*, 9673–9689.

Zipser, E., Liu, C., Cecil, D., Nesbitt, S. W., & Yorty, S. (2006). Where are the most intense thunderstorms on Earth? *Bulletin of the American Meteorological Society*, *87*, 1057–1071.